Journal of the Australian Ceramic Society (2024) 60:471–484
https://doi.org/10.1007/s41779-024-01005-x

RESEARCH

Investigation of the effects of titanium oxide concentration on the sinterability, microstructural characteristics, mechanical properties, in vitro bioactivity, and cell culture behavior of chicken-derived hydroxyapatite

Hasan Gökçe[1]

Received: 12 October 2023 / Revised: 1 February 2024 / Accepted: 10 February 2024 / Published online: 20 February 2024
© The Author(s) 2024

Abstract
This study focuses on how titanium oxide (TiO_2) in concentrations ranging from 0.5 to 4% by weight added the hydroxyapatite (CHA) made from chicken femur bones', affects sinterability, microstructural, mechanical, and in vitro bioactivity properties. According to the results of the experiments, it was determined that CHA decomposed into whitlockite, alpha tricalcium phosphate (α-TCP), tetracalcium phosphate (TTCP), and calcium oxide (CaO) phases at different temperatures. Rutile and perovskite ($CaTiO_3$) phases were also found in TiO_2 added CHAs in addition to these phases. With increasing sintering temperature of CHA, the diameters and the heights of the samples decreased. Density increased up to 1250 °C and decreased at 1300 °C respectively. while the partial density value showed similar behavior with density and hardness, At 1200 °C, the maximum values of fracture toughness (1.071 $MPam^{1/2}$) and compressive strength (145.417 MPa) were attained; however, as sintering temperatures increased, these values shifted downward to 0.882 $MPam^{1/2}$ and 111.096 MPa, respectively. It has been determined that grain growth and decomposition are the underlying factors in obtaining the highest density, hardness, fracture toughness and compressive strength values for CHA at different temperatures. Among the TiO_2 added CHAs, the best properties are obtained for CHA-0.5TiO_2 sintered at 1300 °C (Density: 3.0057 g/cm3, Hardness: 3.973 GPa, Fracture toughness: 1.583 $MPam^{1/2}$ and Compressive strength: 170.045 MPa) and the properties of the CHA-TiO_2 composite decreased with increasing TiO_2 ratio. This is due to the fact that increasing TiO_2 has a detrimental impact on CHA's sinterability behavior and causes it to become more porous and degrade more quickly. It was discovered through in vitro bioactivity and cell culture assays that the addition of TiO_2 had a detrimental impact on the proliferation of bone tissues.

Keywords In vitro bioactivity and cell culture · Chicken hydroxyapatite · Titanium oxide · Sintering

Introduction

Development of biomaterials for the repair/replacement of hard tissue has earned much interest in the past few years, although the conventional method of using autogenous or allogenic bone was most preferred for the treatment of bone defects, disadvantages including, the limited quantity and the risk of transmission of infection (e.g., HIV, hepatitis). Therefore, the development of bone restorative materials with both higher biocompatibility and sufficient mechanical strength is strongly desired. Hydroxyapatite (HA) is one of the most used material in bone regeneration because mainly of its affinity to bone tissues and has a similar chemical and crystallographic structure to the bone mineral [1]. It does not cause any stimulating and repulsive effects when added into the human body. Moreover, HA can combine with the original bone tissue to form a solid bone. It can be synthesized chemically or extracted from biological sources. Biological HA contains different kinds of cationic and anionic impurities. These ionic impurities in biological HAs could be a reason for its better biocompatibility than synthetic HAs [2]. Therefore, many works have been devoted to the development of HA from biological sources like turkey bones [3], goat bones [4], sheep bones [5], and bovine bones [6].

✉ Hasan Gökçe
gokceh@itu.edu.tr

[1] Prof. Dr. Adnan Tekin Materials Science and Production Technologies Applied Research Center (ATARC), Istanbul Technical University, 34469, Maslak, Istanbul, Türkiye

To meet the world's food demands, thousands of tons of chickens are slaughtered each year, and the majority of the leftover bones are dumped in the natural environment. The strongest issues could, however, arise from the release of chicken bones into the environment. It is crucial that this adverse effect appears. Recycling used chicken bones is one method for doing this. The conversion of leftover chicken bones into hydroxyapatites serves this goal [7, 8]. There are two methods for generating hydroxyapatite from chicken bones. The first of these involves washing the precipitated hydroxyapatite particles with distilled water three times after 24 h and drying them in a vacuum oven at 60 °C for 24 h. Waste chicken femur bones are dissolved in ChCl-urea at 100 °C for four hours, then this process is cooled to about room temperature. It was found that the hydroxyapatite (CHA) obtained from chicken bones with this method was in rod-like form, and the pertinent method was unable to produce CHA at a high efficiency [9]. Production through calcination is the second technique. Preventing animal-related health issues and adjusting these inputs with other techniques can both lead to higher efficiency. It has been determined that CHA can be produced at different calcination temperatures and durations as follows in the literature: 1000 °C for ½ hour [10], 950 °C for 2 h [11], 900 °C for 6 h [12], 700 °C for 2 h [13], 600 °C for 2 h [14], 600 °C for 4 h, 12 h, and 20 h [15], and 500 °C for 24 h [16]. However, as can also be seen in Table 1, its low mechanical properties make it unsuitable for use in the human body, and there is only one study in the literature aimed at improving the mechanical properties of CHA. In this study [17], glass addition was employed to enhance the mechanical properties of CHA. However, it was not possible to achieve compressive strength (100–230 MPa), hardness (4.87 GPa), and fracture toughness (2–12 $MPam^{1/2}$) values suitable for use in the human body [18].

Table 1 The data of the study related to the addition of glass to CHA and CHA existing in the literature [17]

Temperature (°C)	Features	CHA	CHA-5 (%wt.) glass	CHA-10(%wt.) glass
1000	Density (g/cm^3)	2.22	2.28	2.25
1100		2.38	2.53	2.45
1200		2.70	2.78	2.72
1300		2.83	2.35	2.06
1000	Hardness	101.4	106	104
1100		171	185	173
1200		222.8	293	258
1300		360	424	467
1000	Compressive strength (MPa)	40.2	48	44
1100		63.2	71	65
1200		66.9	76	68
1300		78.8	41	32

It has been determined that the addition of TiO_2 contributes to the cell proliferation of the HA-Ag binary system [19]. Furthermore, the presence of Ti–OH groups on the TiO_2 surface is associated with a high bioactive response, making it a potential biomaterial[19]. These groups induce protein binding, facilitating cellular adhesion, and are also associated with the nucleation of calcium phosphate when immersed in a solution with a composition similar to blood plasma (SBF). The addition of 11 mol% titanium to a bioactive glass has been found to enhance bioactivity and accelerate apatite formation. A study involving pigs reported that titanium implants coated with titanium nanotubes showed increased bone formation compared to unmodified surface implants, and they exhibited greater gene expression related to bone remodeling and formation [20, 21]. Due to this effect, the impact of synthetic HA [22] and HA obtained from biological sources such as bovine HA [23] and sheep HA [24] on their physical, mechanical, and/or bioactivity properties has been investigated. However, there is no study in the literature regarding its addition as an additive material to CHA.

In this study, hydroxyapatite was produced from chicken femur bones, and the effects of titanium oxide addition at weight ratios of 0.5%, 1%, 2%, and 4% on the properties of chicken hydroxyapatite were investigated.

Materials and methods

As the matrix material, hydroxyapatite (CHA) was created using chicken femur bones from the Erpiliç Company in Istanbul, Turkey, and was produced as follows: The heads of chicken femur bones were cut off to remove visible tissues and substances on the surface, and the marrow in the shafts of all bones was removed by boiling them in water in a pressure cooker for 4 h. After boiling, the remaining shafts were deprotected with sodium hydroxide (NaOH) for 1 h, followed by washing with distilled water, and then calcined at 800 °C for 4 h at heating rates of 5 °C/min. To compare the calcined chicken bones with other bioderived HAs mentioned in the literature, their grain size was increased to -63 by pounding them in a ceramic mortar. Following this stage, titanium oxide (TiO_2; Nanolab, spherical form, average 5 µ) additions were made at weight ratios of 0.5%, 1%, 2%, and 4% and the prepared mixtures were homogenized using a Retsch PM 100 planetary ball mill with 15 zirconia balls and a sufficient amount of ethyl alcohol at a speed of 180 revolutions per minute for 2 h. After the homogenization process, the prepared mixtures were first dried and then pelletized using a uniaxial pressing method under a pressure of 350 MPa to conform to the British 7253

standard. Subsequently, they were sintered at temperatures of 1100, 1150, 1200, 1250, and 1300 °C for 4 h each. Phase investigations of the sintered samples were performed using a Panalytical Expert Pro Series XRD, with Cu-Kα radiation (λ = 0.154 nm, 45 kV and 40 mA), 2θ range of 20–60◦, step size of 0.02◦ and rate of 2◦/min. A Zeiss-Evo | MA10 SEM was used to measure microstructural changes associated to the sintering temperatures and additives made. Measurements of the density, porosity, and partial density were taken, along with measurements of the diameter, length, and volume shortening rates and the physical properties. To calculate the diameter, length, and volume shortening rates, formulas 1, 2, and 3 were employed.

$$S_d = \left(\frac{D_0 - D_1}{\Delta_0}\right) \times 100 \quad (1)$$

S_d: Diameter shrink (%), D_o: Diameter before sintering (mm), D_1: Diameter after sintering (mm)

$$s_l = \left(\frac{L_0 - L_1}{L_0}\right) \times 100 \quad (2)$$

S_l: Shortening in height (%), L_o: Length before sintering (mm), L_1: Length after sintering (mm)

$$s_v = \left(\frac{V_0 - V_1}{V_0}\right) \times 100 \quad (3)$$

S_v: Volumetric shortening (%), V_o: Volume before sintering (mm^3), V_1: Volume after sintering (mm^3).

The Archimedes method was used to determine density, porosity and partial density values and calculations were made according to Formulas 4, 5 and 6. Theoretical densities were determined according to the mixing rule.

$$d = \frac{W_D}{W_a - W_S} \quad (4)$$

Table 2 Change in physical properties of CHAs with and without TiO2 addition depending on sintering temperatures

Temp. (°C)	Property	CHA	CHA-0.5 T	CHA-1.0 T	CHA-2.0 T	CHA-4.0 T
1100	Shrinkage in diameter (%)	9.777 ± 0.744	6.812 ± 0.466	6.088 ± 0.402	4.367 ± 0.157	3.882 ± 0.877
1150		13.432 ± 0.737	11.480 ± 0.485	10.892 ± 0.383	9.192 ± 0.543	7.331 ± 0.514
1200		16.598 ± 0.305	15.009 ± 0.298	14.672 ± 0.358	12.617 ± 0.732	10.491 ± 0.543
1250		17.354 ± 0.524	16.808 ± 0.382	16.190 ± 0.409	15.189 ± 0.643	13.128 ± 0.500
1300		17.591 ± 0.524	17.627 ± 0.554	17.156 ± 0.947	14.561 ± 0.431	13.790 ± 0.589
1100	Shrinkage in length (%)	9.902 ± 1.398	6.394 ± 0.182	6.238 ± 0.181	4.405 ± 0.232	3.696 ± 0.969
1150		12.721 ± 1.011	10.786 ± 0.517	10.467 ± 0.238	8.341 ± 0.463	7.366 ± 0.900
1200		15.548 ± 0.343	14.518 ± 0.432	14.186 ± 0.225	12.501 ± 0.765	10.609 ± 0.776
1250		16.003 ± 0.601	16.426 ± 0.741	15.195 ± 0.781	14.733 ± 0.575	13.611 ± 0.637
1300		16.732 ± 0.749	17.738 ± 0.600	16.747 ± 0.765	14.886 ± 0.912	14.703 ± 0.740
1100	Shrinkage in volüme (%)	26.627 ± 3.063	18.571 ± 2.207	17.438 ± 1.993	12.567 ± 2.151	11.020 ± 1.950
1150		34.585 ± 1.606	30.092 ± 0.876	28.907 ± 0.764	24.419 ± 1.303	20.443 ± 1.528
1200		41.256 ± 0.562	38.251 ± 0.675	37.520 ± 0.566	33.182 ± 1.338	28.382 ± 0.878
1250		42.626 ± 0.854	42.160 ± 0.605	39.741 ± 1.598	37.866 ± 0.969	34.803 ± 0.939
1300		43.447 ± 1.020	43.523 ± 0.730	43.373 ± 2.531	38.667 ± 1.635	36.604 ± 1.241
1100	Density (g/cm^3)	2.301 ± 0.048	2.083 ± 0.039	2.031 ± 0.056	2.020 ± 0.070	2.016 ± 0.103
1150		2.521 ± 0.038	2.399 ± 0.030	2.346 ± 0.025	2.318 ± 0.009	2.173 ± 0.005
1200		2.807 ± 0.007	2.772 ± 0.050	2.715 ± 0.036	2.610 ± 0.049	2.448 ± 0.078
1250		2.973 ± 0.034	2.932 ± 0.016	2.838 ± 0.020	2.812 ± 0.062	2.685 ± 0.027
1300		2.964 ± 0.012	3.005 ± 0.017	2.990 ± 0.018	2.692 ± 0.073	2.548 ± 0.027
1100	Porosity (%)	23.798 ± 3.011	33.603 ± 1.216	34.249 ± 1.452	35.313 ± 2.012	35.637 ± 3.971
1150		17.094 ± 1.221	23.300 ± 0.832	25.644 ± 0.816	26.237 ± 0.278	31.259 ± 0.501
1200		5.501 ± 0.546	8.835 ± 0.924	11.089 ± 0.614	15.705 ± 2.352	22.113 ± 2.850
1250		3.237 ± 0.055	2.796 ± 0.948	6.273 ± 1.036	9.012 ± 2.188	14.386 ± 1.664
1300		1.790 ± 0.038	1.354 ± 0.445	1.675 ± 0.484	13.231 ± 2.487	18.816 ± 1.032
1100	Relative density (%)	72.934 ± 1.521	65.353 ± 1.236	63.956 ± 1.468	63.938 ± 2.209	62.497 ± 2.242
1150		79.905 ± 1.205	75.927 ± 0.977	73.983 ± 0.802	73.277 ± 0.287	68.184 ± 2.441
1200		88.966 ± 0.248	87.728 ± 1.586	85.823 ± 1.154	82.288 ± 1.558	76.798 ± 2.453
1250		94.202 ± 1.251	92.789 ± 0.531	89.697 ± 0.654	88.669 ± 1.985	84.213 ± 0.856
1300		93.929 ± 0.397	95.119 ± 0.553	94.501 ± 0.597	84.894 ± 2.331	79.945 ± 0.847

Table 3 Change of mechanical properties of CHA and CHA-TiO_2 composites depending on sintering temperatures

Temp. (°C)	Property	CHA	CHA-0.5 T	CHA-1.0 T	CHA-2.0 T	CHA-4.0 T
1100	Hardness (GPa)	0.752 ± 0.046	0.623 ± 0.128	0.631 ± 0.108	0.564 ± 0.071	0.486 ± 0.022
1150		2.251 ± 0.192	1.380 ± 0.107	1.249 ± 0.110	0.878 ± 0.073	0.720 ± 0.051
1200		3.923 ± 0.305	2.266 ± 0.120	2.129 ± 0.224	1.507 ± 0.135	0.958 ± 0.116
1250		4.354 ± 0.331	3.268 ± 0.249	2.807 ± 0.219	2.185 ± 0.360	1.683 ± 0.135
1300		4.321 ± 0.189	3.973 ± 0.260	3.260 ± 0.414	2.313 ± 0.245	1.757 ± 0.185
1100	Fracture toughness ($MPam^{1/2}$)	0.489 ± 0.031	0.710 ± 0.001	0.704 ± 0.003	0.680 ± 0.048	0.667 ± 0.133
1150		0.705 ± 0.173	0.986 ± 0.094	0.969 ± 0.113	0.857 ± 0.106	0.832 ± 0.100
1200		1.071 ± 0.184	1.285 ± 0.151	1.117 ± 0.093	1.067 ± 0.025	0.930 ± 0.013
1250		0.928 ± 0.137	1.446 ± 0.084	1.385 ± 0.057	1.352 ± 0.157	1.197 ± 0.012
1300		0.882 ± 0.058	1.583 ± 0.277	1.408 ± 0.241	1.188 ± 0.184	0.899 ± 0.171
1100	Brittleness Index ($\mu^{-1/2}$)	1.538 ± 0.095	0.877 ± 0.180	0.897 ± 0.192	0.830 ± 0.488	0.728 ± 0.165
1150		3.193 ± 0.272	1.400 ± 0.103	1.289 ± 0.967	1.024 ± 0.691	0.865 ± 0.118
1200		4.034 ± 0.309	1.763 ± 0.093	1.906 ± 0.392	1.411 ± 0.363	1.030 ± 0.300
1250		4.227 ± 0.328	2.260 ± 0.172	2.025 ± 0.380	1.615 ± 0.291	1.405 ± 0.350
1300		4.936 ± 0.215	2.509 ± 0.164	2.314 ± 0.308	1.946 ± 0.330	1.953 ± 0.325
1100	Compression strength (MPa)	71.154 ± 6.082	69.061 ± 4.358	60.008 ± 4.582	53.267 ± 7.549	40.963 ± 4.358
1150		124.343 ± 6.557	87.004 ± 4.802	82.068 ± 12.288	55.325 ± 13.000	47.432 ± 10.000
1200		145.417 ± 5.000	112.044 ± 7.810	98.048 ± 8.185	95.843 ± 9.165	81.528 ± 8.888
1250		139.648 ± 4.557	114.096 ± 5.196	108.297 ± 10.583	107.538 ± 6.244	104.379 ± 7.000
1300		111.096 ± 9.643	170.045 ± 5.656	157.483 ± 6.082	128.642 ± 5.000	106.584 ± 7.000

$$p = \left(\frac{w_D - w_a}{w_D - w_S}\right) \times 100 \tag{5}$$

$$R_d = \left(\frac{d}{d_t}\right) \times 100 \tag{6}$$

d: Density (g/cm^3), p: Porosity (%), R_d: Partial density (%), d_t: Theoretical density (g/cm^3), W_D: Dry weight (gr), W_a: Suspended weight (gr), W_s: Weight in water (gr).

Hardness, fracture toughness and compressive strength tests were performed to determine the mechanical properties. Future Tech FM300 brand hardness device was used to find the hardness and fracture toughness values, and the samples were sanded with 600, 800, 1000, 1200, 2400, 4000 and 5000 mesh sandpapers, respectively, before the relevant measurements. In order to determine the fracture toughness values, polishing processes were carried out using 5 µ, 3µ, 1µ and 0.5µ diamond pastes after sanding processes. The hardness values were calculated using Formulas 7 and 8, respectively, with loads of 200 g (20 s) and 300 g (10 s), respectively. Compressive strength test 2 mm/min. It was carried out on a Devotrans 50kN brand universal testing device at speed and determined using Formula 9. The fragility index was calculated from the HV/K_{ic} ratio [25].

$$HV = 0.0018544(P/d^2) \tag{7}$$

HV: Hardness value (GPa), *P:* Applied force (N), d: Average track diameter (mm^2)

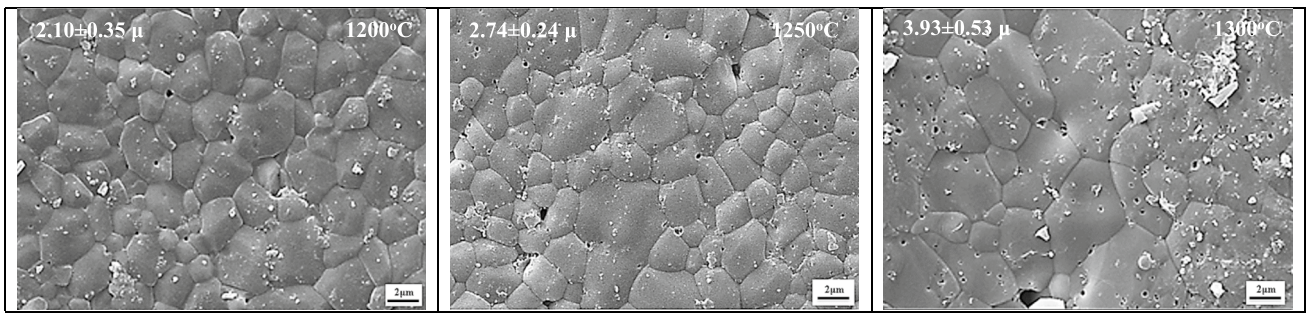

Fig. 1 SEM microstructure images of CHA sintered at 1200, 1250 and 1300 °C

Table 4 Properties of HA and TiO_2

Properties	HA [50]	TiO_2 [51]
Compressive Strength (MPa)	300–900	660–3675
Elasticity Modulus (GPa)	80–120	288
Fracture Toughness ($MPam^{1/2}$)	0.6–1	3.3
Density (g/cm^3)	3.156	4.23

$$K_{ic} = 0.203(c/a)^{-1.5}(HV)(a)^{0.5} \quad (8)$$

K_{ic}: Fracture toughness ($MPam^{1/2}$), c = Distance of the crack formed from the center of the microhardness mark (m), HV: Hardness (MPa), a: Half of the mark formed in microhardness measurement (m)

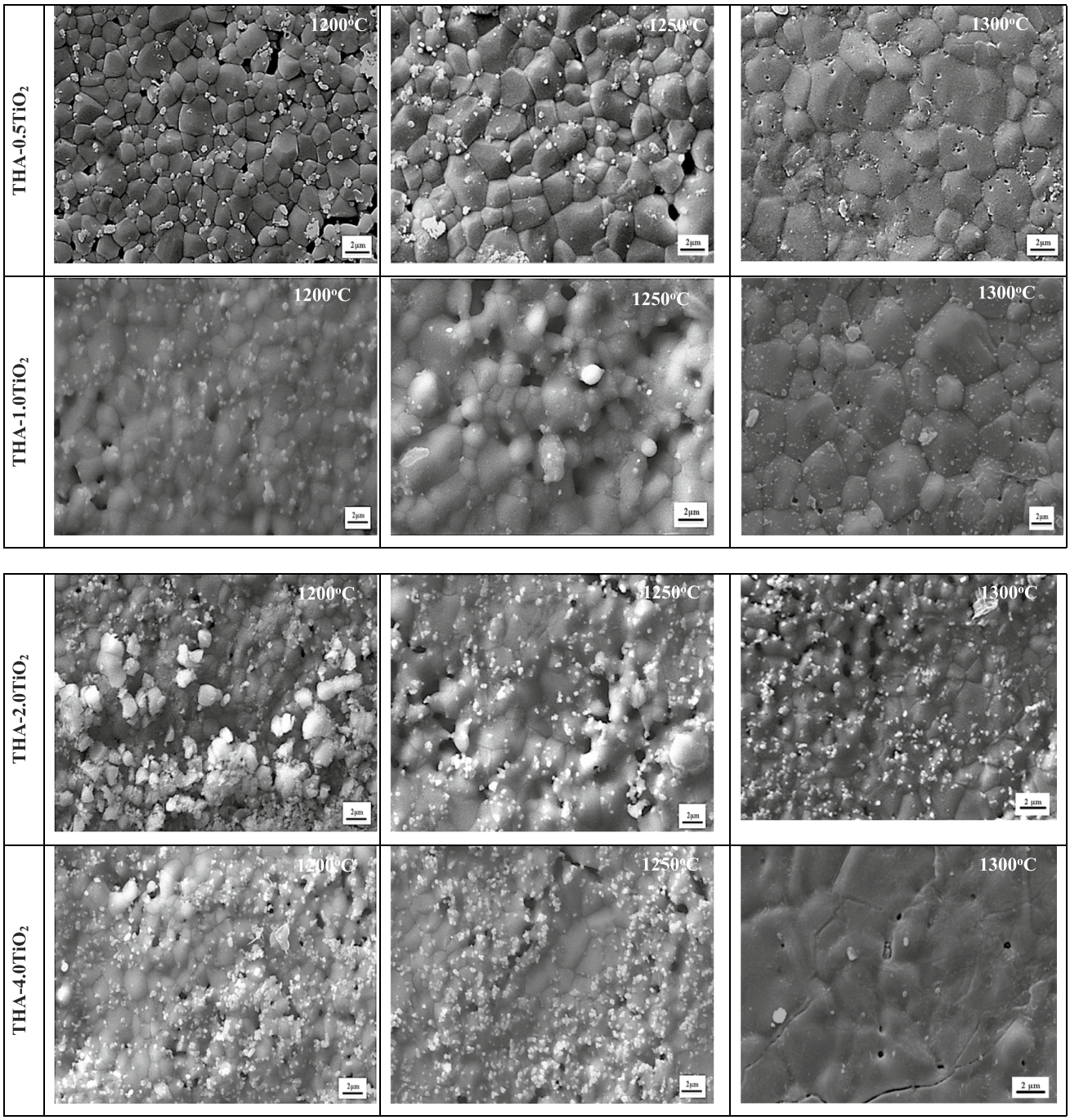

Fig. 2 SEM microstructure images of CHA-TiO_2 composites sintered at 1200, 1250 and 1300 °C temperatures

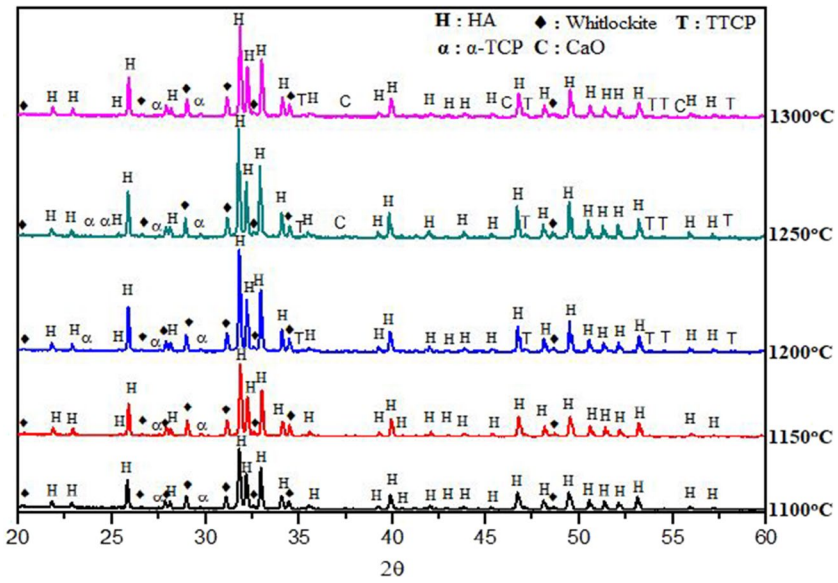

Fig. 3 XRD analysis of pure CHA depending on increasing sintering temperatures

Table 5 Chemical composition of CHA determined by Rietveld analysis depending on sintering temperatures

Sintering temperature (°C)	Chemical composition (%)				
	HA	Whitlockite	α-TCP	TTCP	CaO
1100	83.7	15.9	0.4	0	0
1150	81.1	18.6	0.3	0	0
1200	79.1	19.8	0.4	0.7	0
1250	75.6	20.6	1.6	2.1	0.1
1300	74.9	20.2	1.9	2.8	0.2

$$\sigma_C = \frac{F}{A_0} \tag{9}$$

$\sigma_{c:}$ Compressive strength (MPa), F: Maximum force (N), A_o: Cross-sectional area (mm^2).

For the in vitro test, totally, two samples were sintered to the temperatures in which they attained the highest compressive strength value with the size of ∅11 and 4 mm^2. After this stage, the samples were ground by 400, 600, 800, 1000, and 1200 mesh SiC paper and then they were dried in an oven at 105 °C for 1 day. The samples were immersed in sealed test tubes containing 20 mL of SBF for 14 and

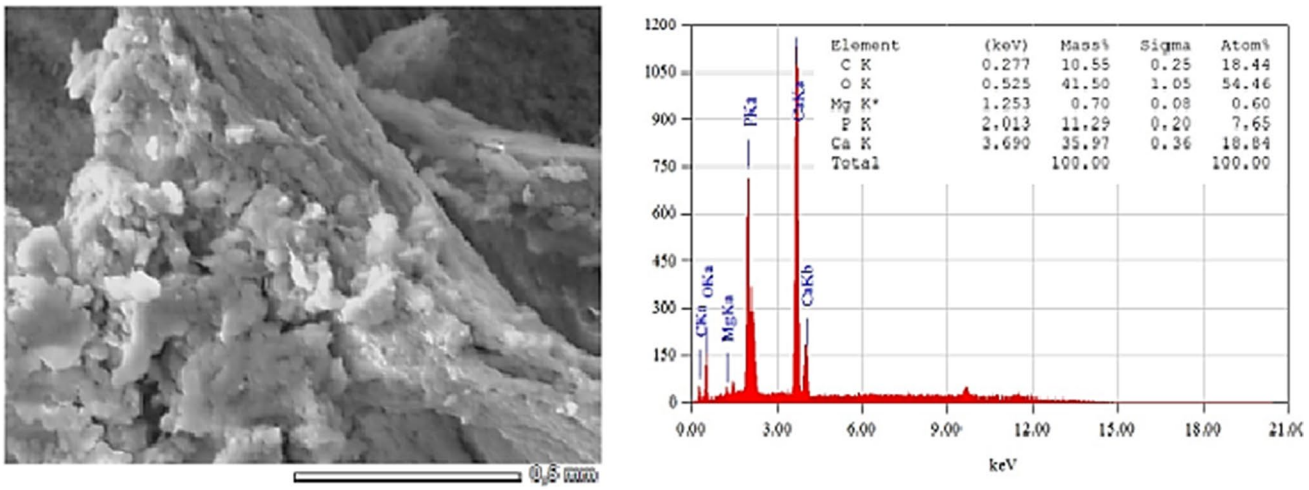

Fig. 4 EDS analysis of chicken femur bone calcined at 800 °C for 2 h

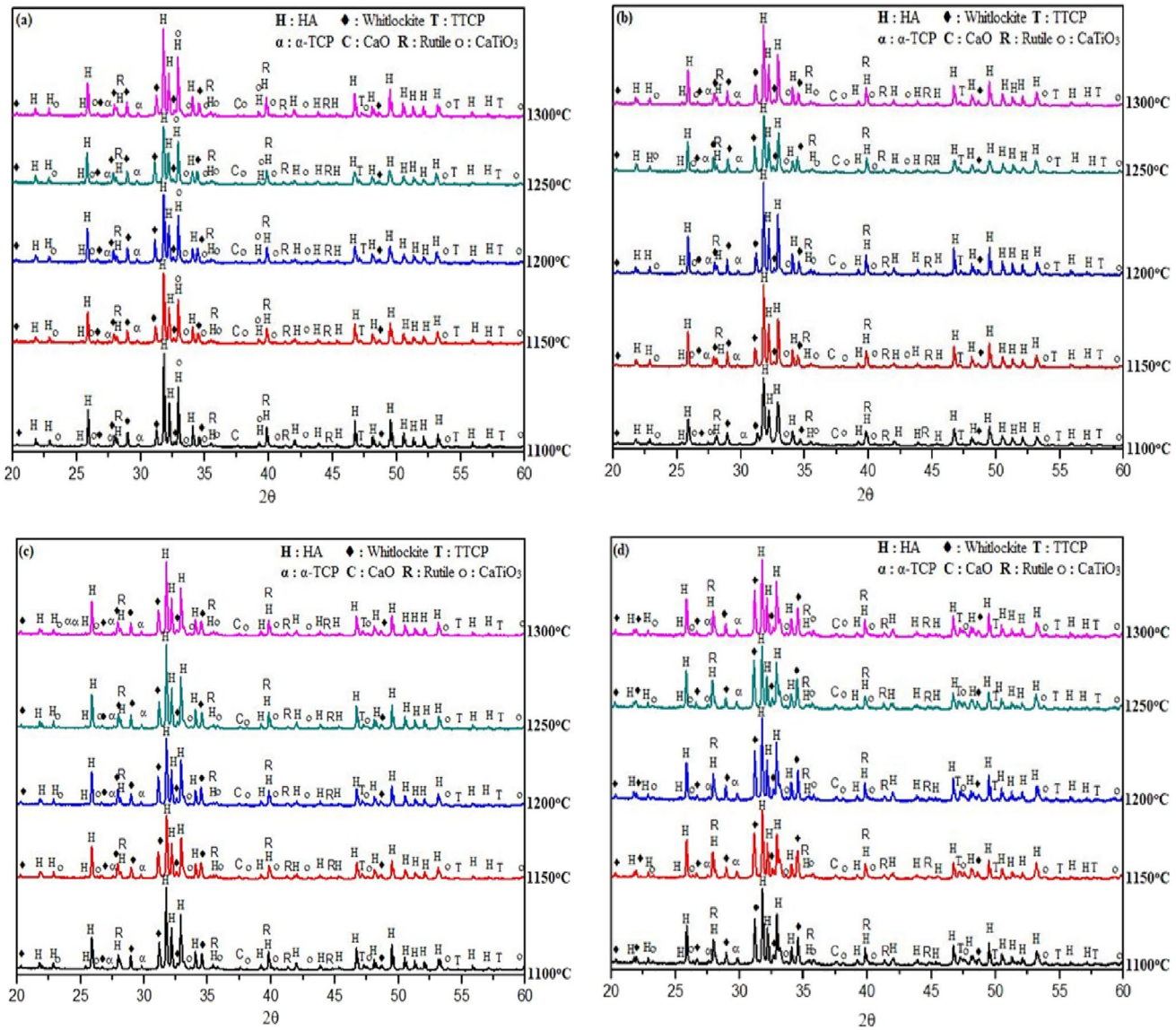

Fig. 5 XRD analyzes of CHA- (**a**) 0.5, (**b**) 1, (**c**) 2 and (**d**) 4 TiO_2 composites due to increasing sintering temperatures

21 days. The 20-mL SBF solutions used in the in vitro tests were refreshed every day until the specified times were completed. When the specified times were completed, the samples were taken from SBF solutions without damaging the apatite layers and then cleaned by distilled water and finally dried at 60 °C for 12 h. Apatite layers occurring on the surface of the samples immersed in SBF solutions were investigated by SEM [26]. For cell culture tests, 3T3 mouse embryonic fibroblast cell line was provided by American Type Culture Collection and was grown in monolayer culture in Dulbecco's Modified Eagle's Medium supplemented with 10% heat-inactivated fetal bovine serum and 1%penicilin–streptomycine antibiotic mixtures at 37 °C with 5% CO_2 and 95% humidity. Trypsin/EDTA0.25% solution was used to remove cells from the culture flask. Cells were reseeded at a density of 1×10^5 cells into the 25 T flasks. For SEM analysis, samples and glass cover slip were placed into the 6-wells culture plates containing of 5 ml completed DMEM medium and then 3T3 cells were seeded with the concentration of 5×10^4 cells/well for 7 days. The glass cover slip and samples were critical-point dried and mounted on appropriate stubs with carbon tape and sputter-coated with gold. Images were collected using a SEM [27].

Results & discussion

According to the sintering temperatures, Table 2 illustrates how the physical characteristics of CHAs with and without TiO_2 addition change. With increasing temperature,

Table 6 Chemical composition of CHA-TiO_2 composites

Sintering temperature (°C)	Sample ID	Chemical composition (%)						
		HA	Whitlockite	α-TCP	TTCP	CaO	Rutile	$CaTiO_3$
1100	CHA-0.5 T	78.9	20.0	0.3	0.1	0.1	0.2	0.4
1150		76.6	22.2	0.4	0.1	0.1	0.2	0.4
1200		74.5	24.2	0.5	0.1	0.1	0.2	0.4
1250		71.9	23.8	0.8	2.8	0.1	0.2	0.4
1300		69.9	25.0	1.3	3.1	0.1	0.2	0.4
1100	CHA-1.0 T	73.5	24.2	0.5	0.7	0.1	0.4	0.6
1150		71.7	25.2	0.6	1.4	0.1	0.4	0.6
1200		70.4	25.9	0.9	1.7	0.1	0.4	0.6
1250		66.1	27.6	1.3	3.9	0.1	0.4	0.6
1300		63.8	29.3	1.0	4.8	0.1	0.4	0.6
1100	CHA-2.0 T	67.2	27.1	1.7	1.9	0.1	0.7	1.3
1150		65.2	27.4	3.1	2.1	0.2	0.7	1.3
1200		63.8	27.8	2.6	3.4	0.4	0.7	1.3
1250		61.6	28.4	3.5	4.4	0.5	0.7	1.3
1300		59.3	29.1	4.3	5.2	0.6	0.7	1.3
1100	CHA-4.0 T	63.3	27.8	2.2	2.4	0.3	1.1	2.9
1150		61.7	28.1	2.8	2.9	0.5	1.1	2.9
1200		59.0	28.6	3.7	3.9	0.8	1.1	2.9
1250		56.5	29.2	4.6	4.8	0.9	1.1	2.9
1300		54.0	29.7	5.4	5.9	1.0	1.1	2.9

the diameter reduction rate of CHA has increased from 9.777 to 17.591% the length reduction rate from 9.902% to 16.732% and the volume reduction rate from 26.627% to 43.447% These ratios are compatible with waste bovine HA [28] and synthetic HA [29]. The sample sintered at 1300 °C with a 0.5% TiO_2 addition had the maximum diameter, length, and volume reduction rates that belonged to pure CHA. The diameter reduction rate dropped as the TiO_2 ratio increased, as did the length reduction rate from 17.738% to 14.703% and the volume reduction rate from 43.523% to 36.604%. The highest density and partial density values for CHA were achieved at 1250 °C, but at 1300 °C, they decreased from 2.973 g/cm^3 to 2.964 g/cm^3 and from 94.202to 93.929, respectively. As expected, the porosity ratio decreased with increasing temperature. In the CHA-TiO_2 composites, density values increased with increasing temperature for CHA-0.5 T and CHA-1.0 T. However, the highest densities for CHA-2.0 T and CHA-4.0 T composites were achieved during sintering at 1250 °C, with values of 2.812 g/cm^3 and 2.685 g/cm^3, respectively. Sintering these composites at 1300 °C caused a decrease in density values to 2.629 g/cm^3 and 2.548 g/cm^3, respectively. The partial density values of CHA-TiO_2 composites exhibited similar behavior to their density counterparts. The highest partial density was measured in the CHA-0.5 T composite at 95.119%, while the lowest partial density was observed in the CHA-4.0 T composite at 79.945%. The porosity ratios decreased with increasing temperature for CHA-0.5 T and CHA-1.0 T composites. As for CHA-2.0 T and CHA-4.0 T composites, the lowest porosity ratios were measured at 1250 °C, at 9.012% and 14.386%, respectively. The sintering of these composites at 1300 °C resulted in an increase in the porosity. There are several reasons why CHA-2.0 T and CHA-4.0 T composites exhibit lower physical properties compared to both CHA and CHA-0.5 T and CHA-1.0 T composites: Firstly, due to the higher melting temperature of TiO_2 (1840 °C [30]) compared to HA (1614 °C [31]), the increased sintering behavior with increasing TiO_2 content decreases [32]. Secondly, the increased TiO_2 content leads to an increased rate of decomposition in CHA-TiO_2 composites. Similar behavior has been observed in synthetic HA [33] and HA derived from biological sources [34]. Thirdly, the thermal expansion coefficients of the detected Rutile ($11.1 \times 10–6$/°C [35]) and $CaTiO_3$ ($12.9 \times 10–6$/°C [36]) phases in CHA-TiO_2 composites are incompatible with HA ($13.6 \times 10–6$/°C [37]). Fourthly, in HA-TiO_2 composites, when the contribution of TiO_2 to the physical and mechanical properties is less than 2%, it is because the presence of 2% or more TiO_2 exceeds the solubility limit within HA, leading to an increase in the decomposed ratio of HA along with an increase in the proportion of $CaTiO_3$ [38]. For this reason, as can be seen in Table 3, the mechanical properties of CHA-2.0 T and CHA-4.0 T composites are less than CHA-0.5 T and CHA-1.0 T composites.

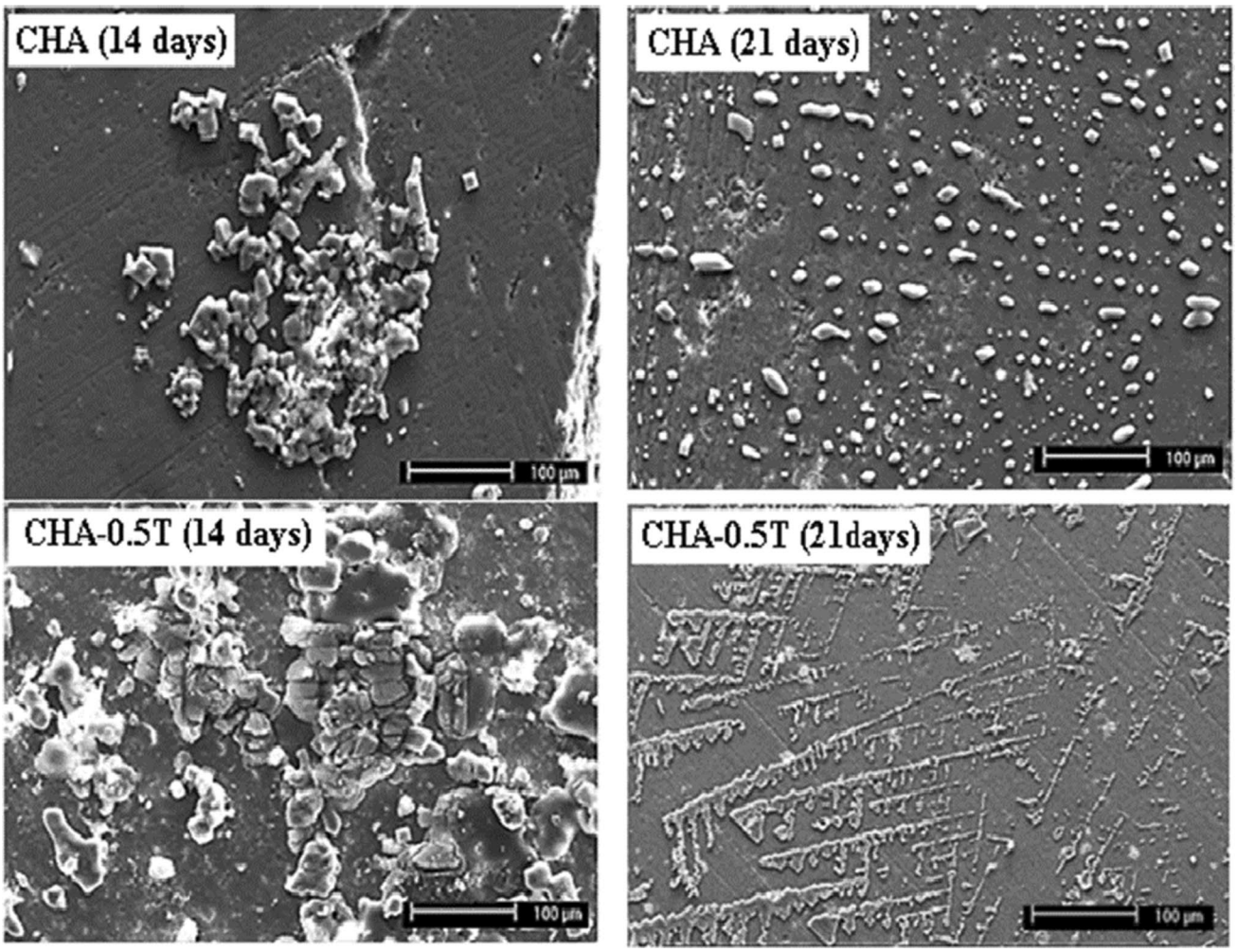

Fig. 6 SEM microstructures of CHA and CHA-0.5 T composite immersed in SBF solution for 14 and 21 days

Table 3 shows the change of mechanical properties of CHA and CHA-TiO_2 composites depending on sintering temperatures. The hardness of CHA increased up to 1250 °C and increased from 0.752GPa to 4.354GPa, but; It was stretched to 4.321GPa at 1300 °C. Similar behavior was also confirmed by Ramesh et al. [39]. This is due to the fact that the rate of total decomposes increased at 1300 °C compared to 1250 °C [40]. At 1200 °C, CHA had the greatest measured fracture toughness and compressive strength, which were $1.071 \pm \text{MPam}^{1/2}$ and 145.417 ± 5.000 MPa, respectively. However, both properties decreased with increasing temperature. The highest fracture toughness of CHA is compatible with HA ceramics [41–43]. There are two reasons for the decrease in fracture toughness and compressive strength for CHA: First; As can be seen in Fig. 1, it is the increase in grain size in CHA sintered at 1250 °C and 1300 °C. The second reason is related to the increased decomposition of CHA into secondary phases such as α-TCP, TTCP, and CaO. This increase leads to the formation of gas voids within CHA [44, 45].

Although increasing the average grain size may cause an increase in the shortening rate, density and/or hardness of HA ceramics, it also causes a decrease in their compressive strength. As can be seen in Eq. 1 and commonly observed in ceramics, the strength increases as the porosity, p, decreases. (σ: Compressive strength (MPa), σ_o: Compressive strength of non-porous HA (MPa), b: Material constant, p: Pore amount)

$$\sigma = \sigma_o \exp(-bp) \tag{E.1}$$

However, as can be observed from Eq. 2, once the average particle size and the rate of decompose in HA ceramics beyond a certain point, the compressive strength decreases with temperature.

$$\sigma = kd^{-1/2} \tag{E.2}$$

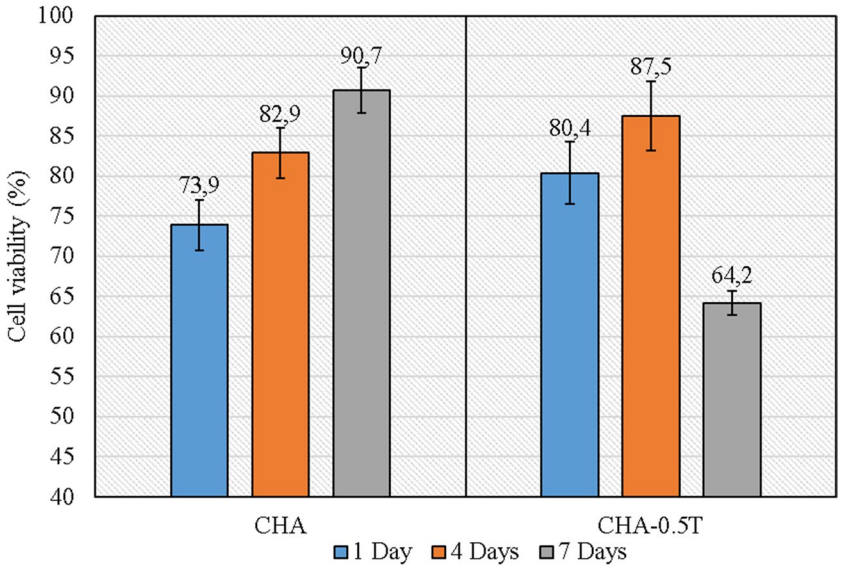

Fig. 7 Cell rate on the surface of CHA and CHA-0.5 T composite subjected to cell culture testing for 1, 4 and 7 days

Here k: material constant, d is the average grain size [46].

The brittleness index increased with increasing temperature and increased from 1.538$\mu^{-1/2}$ to 4.936 $\mu^{-1/2}$. The brittleness index for CHA-TiO_2 composites varies between 0.728 and 2.509 $\mu^{-1/2}$. As can be seen from these values, the lowest and highest fragility index values of CHA have been reduced by approximately 50%. This is similar to ref. [47–49] the rate of decrease. The mechanical properties of CHA-TiO_2 composites decreased with increasing TiO_2 content. It is seen that the highest mechanical properties in CHA-TiO2 composites belong to CHA-0.5 T sintered at 1300 °C. For this composite, hardness was calculated as 3.973 GPa, fracture toughness as 1.583 $MPam^{1/2}$ and compressive strength as 170.045 MPa. As can be seen from these values, 47.80% increase in fracture toughness, 16.93% increase in compression strength and 49.16% decrease in brittleness index can be achieved when compared to the highest strength values of CHA. This is the result of TiO_2 having higher mechanical properties to HA, as seen in Table 4.w

The decline in mechanical characteristics of CHA-TiO_2 composites with increasing TiO_2 ratio can be attributed to a number of factors. First, increasing the TiO_2 ratio causes porous structures to emerge, as shown in Fig. 2. Latter; increasing TiO_2 causes an increase in the rate

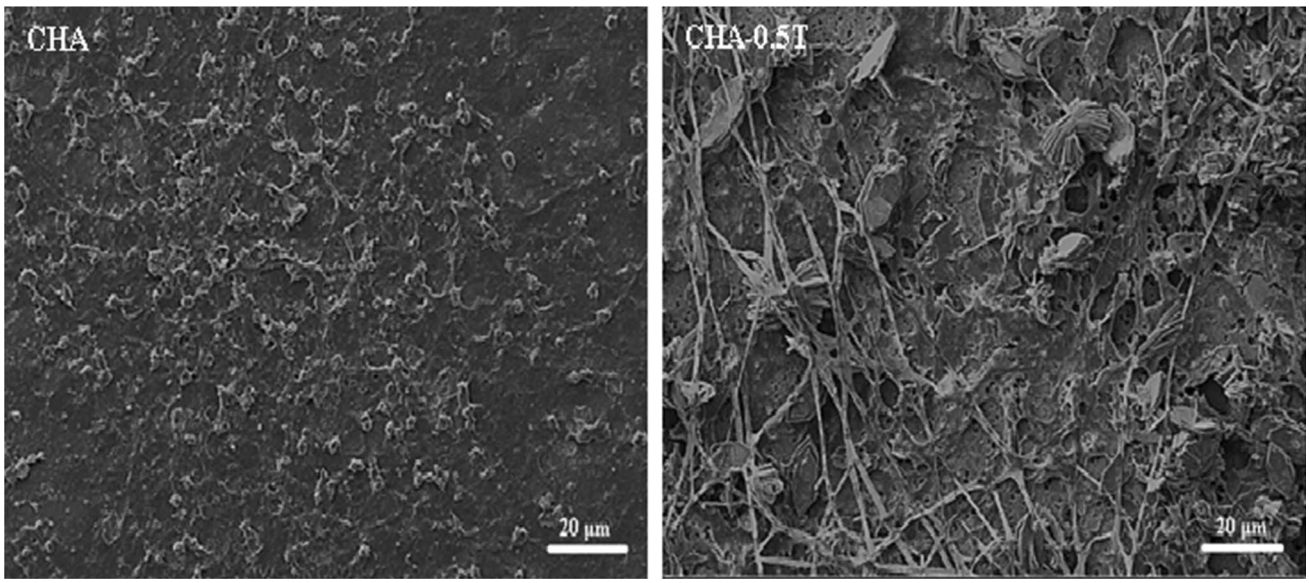

Fig. 8 SEM images of CHA and CHA-0.5 T composite subjected to cell culture testing for 7 days

of decomposition [52]. This rise is the result of a faster rate of phase production in CHA, which produces phases with lower densities than HA. (α-TCP: 2.866 g/cm^3 [53], TTCP: 2.97 g/cm^3 [54]). Third: Rutile and $CaTiO_3$ have better mechanical qualities than -TCP, TTCP, and CaO phases [55, 56].

As a result of XRD analysis of pure CHA, it was determined that CHA decomposed into whitlockite (XRD card number: 98–000-0800) and α-TCP (XRD card number: 98–007-8499) phases for temperatures of 1100 and 1150 °C (Fig. 3). The sintering of pure CHA from 1200 °C resulted in its decomposition into tetracalcium phosphate (TTCP; XRD card number: 98–000-6146) and calcium oxide (CaO; 98–003-4978) phases in addition to whitlockite and α-TCP. According to the sintering temperatures, Table 5 displays the chemical composition of CHA as determined by Rietveld analysis (by using High Score Plus Version 5.2). In CHA, the HA rate dropped from 83.7% to 74.9%. Up to 1250 °C, the proportion of the whitlockite phase grew with rising temperature, but at 1300 °C, it dropped from 20.6% to 20.2%. At this temperature, the ratio of α-TCP, TCP and CaO gases was calculated as 1.9%, 2.8% and 0.2%, respectively. It was noticed that the natural hydroxyapatite started to decompose at temperatures above 700 °C, while CaO occurrence began at a temperature of approximately 800 °C. The presence of CaO in natural HAs continue to temperature of 1100 °C [57], but it is an undesirable phase because it leads to the decohesion and may also alter the rate and extent of biodegradation of sintered HA when implanted in human body [58]. TCP has three polymorphs, such as: β-TCP is stable below 1180 °C, α-TCP between 1180 °C and 1400 °C, and ά-TCP above 1470 °C [59]. The co-existence of TCP phases with HA is recently desired, due to they contribute to the formation of bony tissues on the around of HA implants at a less time compared to monolithic HA [59].

The reason why the whitlockite phase is detected in CHA is due to the Mg found in chicken femur bones (Fig. 4) [50]. A similar formation has also been confirmed in the HAs obtained from tuna [51]and pork [60] found in the literature. The presence of the whitlockite phase contributes to the condensation, biocompatibility and mechanical properties of HA. Apart from this, its solubility in the body is lower than β-TCP [61].

In addition to the phases found in pure CHA, such as HA, Whitlockite, TTCP, -TCP, and CaO, Rutile and $CaTiO_3$ phases were also found in TiO_2 added CHAs, as shown in Fig. 5. It was determined that the intensity of Whitlockite, TTCP, α-TCP and CaO phases detected in pure CHA increased depending on the increasing TiO_2 ratio. In research on HA-TiO_2 composites, it was determined that the decomposition rate of HA into β-TCP increased as the TiO_2 ratio increased and HA decomposed as seen in Reaction 2. [62]. In this study, it was determined that the formation of the β-TCP phase did not occur due to the whitlockite phase. The formation of the $CaTiO_3$ phase occurs due to the decomposition of THA into CaO and the reaction of CaO with TiO_2 as seen in Reaction 3 [63].

$$Ca_{10}(PO_4)_6(OH)_2 + TiO_2 \rightarrow 3Ca_3(PO_4)_2 + CaTiO_3 + H_2O \quad \text{(R.2)}$$

$$CaO + TiO_2 \rightarrow CaTiO_3 \quad \text{(R.3)}$$

While rutile and anatase are formed due to the transformation of TiO_2 around 600 °C, the $CaTiO_3$ phase begins to form in HA-TiO_2 composites starting from 900 °C [64]. The presence of the rutile phase contributes to the increase in the in vitro bioactivity of HA-TiO_2 composites [65].

The chemical composition of CHA-TiO_2 composites is given in Table 6. Depending on the rising TiO_2 ratio in CHA-TiO_2 composites, the rate of HA conversion to secondary phases rises. The secondary phase ratio grew to 46% in the CHA-4.0 T composite from the CHA-0.5 T composite's value of 30.1%. The CHA-4.0 T composite sintered at 1300 °C has the highest breakdown rate among CHA-TiO_2 composites. However, this value is considerably less than the 79% decomposition rate reported by M.A. Monge et al. [66]. The main reason for this is that the secondary phase occurring in CHA is whitlockite.

The SEM microstructures of the in vitro bioactivity CHA and CHA-0.5 T composite are shown in Fig. 6. According to in vitro bioactivity experiments, CHA-0.5 T composite surfaces produce more apatite than CHA does during the course of both the 14-day and 21-day SBF periods. This is due to two factors: The first is related to the type and proportions of phases present in the CHA-0.5 T composite. The fact that the ratio of α-TCP and TTCP phases in the CHA-0.5 T composite was higher than that of CHA increased its in vitro bioactivity. Because the in vitro bioactivity of HA ceramics is increased by the presence of these phases [67]**.** In addition, since these phases are bioabsorbable, they trigger the formation of an apatite layer [68]. Rutile phase accelerates the formation of apatite layer in (100), (110) and (001) directions [69]. The coexistence of $CaTiO_3$ and α-TCP phases facilitates the bone-implant interface interaction and increases the amount of apatite precipitation. The second is; CHA-0.5 T composite has a lower average grain size than CHA. The decrease in average grain size accelerates the precipitation of apatite grains [70].

Figure 7 shows the cell ratio on the surface of CHA and CHA-0.5 T composite subjected to cell culture testing for 1, 4 and 7 days. During cell culture, proteins, mainly extracellular matrix (ECM) proteins adsorb onto material surfaces and the adsorbed proteins help in cell attachment onto material surfaces [71]. It was determined that the CHA-0.5 T composite provided a higher rate of cell formation compared to CHA in 1 and 4-day cell culture tests. In contrast to

CHA, it resulted in a slower rate of cell development after 7 days. A similar situation was also confirmed by Zheng et al. [72]. Figure 8 shows the SEM images of CHA and CHA-0.5 T composite subjected to cell culture testing for 7 days. Although there was a decrease in the number of cells formed on the surface of the CHA-0.5 T composite after 7 days, the typical osteoblast phenotype is healthy cells with some filopodial and lamellipodial extensions. These characteristics indicate that the cells highly adhered and spread onto the surface and suggest the good viability of the cells on the CHA-0.5 T composite [73].

Conclusions

On the basis of experimental results of this investigation, several concluding statements can be made:

In the present study, the potential of TiO_2 on the sintering performance and properties of CHA was evaluated by microstructural and mechanical analyses.

In TiO_2 added CHAs, the maximum size reduction was obtained in 0.5%TiO_2 added sample sintered at 1300 °C.

Depending on the rising TiO_2 ratio in CHA-TiO_2 composites, the rate of HA conversion to secondary phases rises.

It has been determined that grain growth and decomposition are the underlying factors in obtaining variable density, hardness, fracture toughness and compressive strength values for CHA at different and increasing sintering temperatures.

Among the TiO_2 added CHAs, the best properties were obtained in CHA-0.5TiO_2 samples sintered at 1300 °C, and the increased additive ratio negatively affected the properties. The increasing amount of TiO_2 reduces the sintering of CHA and increases the porosity and degradation rate of the structure.

However, as a result of in vitro bioactivity and cell culture tests, it was determined that although TiO_2 addition to CHA was high at first, as the time increased, it negatively affected and decreased the proliferation of bony tissues in the structure.

Funding Open access funding provided by the Scientific and Technological Research Council of Türkiye (TÜBİTAK).

Declarations

Competing interest The authors declare that they have no known competing financial interests or personal relationships that could have appeared to influence the work reported in this paper.

Open Access This article is licensed under a Creative Commons Attribution 4.0 International License, which permits use, sharing, adaptation, distribution and reproduction in any medium or format, as long as you give appropriate credit to the original author(s) and the source, provide a link to the Creative Commons licence, and indicate if changes were made. The images or other third party material in this article are included in the article's Creative Commons licence, unless indicated otherwise in a credit line to the material. If material is not included in the article's Creative Commons licence and your intended use is not permitted by statutory regulation or exceeds the permitted use, you will need to obtain permission directly from the copyright holder. To view a copy of this licence, visit http://creativecommons.org/licenses/by/4.0/.

References

1. Ning, C.Q., Zhou, Y.: On the microstructure of biocomposites sintered from Ti, HA and bioactive glass. Biomaterials **25**, 3379–3387 (2004)
2. Pazarlioğlu, S., Bakdemir, S., Gökçe, H.: Evaluation of the potential of barium zirconate on the sinterability and properties of bovine hydroxyapatite. Ceramics-Silikaty **67**(1), (2004). https://doi.org/10.13168/cs.2023.0009
3. SerdarPazarlioglu, S., Gokce, H., Ozyegin, S., Salman, S.: Effect of sintering on the microstructural and mechanical properties of meleagris gallopova hydroxyapatite. Bio-Med. Mater. Eng. **24**, 1751–1769 (2014). https://doi.org/10.3233/BME-140987
4. Akyurt, N., Yetmez, M., Oktar, F.N.: Studies on goat hydroxyapatite/commercial inert glass biocomposites. J. Aust. Ceram. Soc. **55**, 697–702 (2019). https://doi.org/10.1007/s41779-018-0279-z
5. Demirkol, N., Oktar, F.N., Kayali, E.S.: Mechanical and Microstructural properties of sheep hydroxyapatite (SHA)-niobium oxide composites. Acta Phys. Pol., A **121**(1), 274–276 (2012). https://doi.org/10.12693/APhysPolA.121.274
6. Ayatollahi, M.R., Yahya, M.Y., Shirazi, H.A., Hassan, S.A.: Mechanical and tribological properties of hydro-xyapatite nanoparticles extracted from natural bovine bone and the bone cement developed by nano-sized bovine hydroxyapatite filler. Ceram. Int. **41**, 10818–10827 (2015). https://doi.org/10.1016/j.ceramint.2015.05.021
7. Boutinguiza, M., Pou, J., Comesaña, R., Lusquiños, F., de Carlos, A., León, B.: Biological hydroxyapatite obtained from fish bones. Mater. Sci. Eng. C **32**, 478–486 (2012)
8. Hart, A., Ebiundu, K., Peretomode, E., Onyeaka, H., Nwabore, O.F., Obileke, K.: Value-added materials recovered from waste bone biomass: technologies and applications. RSC Adv. **12**, 22302–22320 (2022)
9. Song, W., Yang, Y., Deng, Y.: Research of preparation conditions for regeneration of hydroxyapatite and influence on crystalline forms. Chem. Ind. **67**, 11–12 (2018)
10. Jorge Humberto, L.D., Héctor, T.J., Heriberto, H.C., Margarita, G.H., José Aaron, M.B., Hakan, N.: Development and in vivo response of hydroxyapatite/whitlockite from chicken bones as bone substitute using a chitosan membrane for guided bone regeneration. Ceram. Int. **44**(18), 22583–22591 (2018)
11. Marzieh, R., Arvydas, P., Ahmad, M., Sohrab, N., Andrius, V., Giedrius, J.: Comparing methods for calculating nano crystal size of natural hydroxyapatite using X-ray diffraction. Nanomaterials **10**(9), 1627 (2020)
12. Hanny, A., Islam, M.R., Sumdani, M.G., Rashidi, N.M.: The effects of sintering on the properties of epoxy composites reinforced with chicken bone-based hydroxyapatites. Polym. Test. **78**, 105987 (2019)
13. Vijayaraghavan, P., Rathi, M.A., Khalid, S.A., Fatima, S.A., Yahya, B.E., Soon, W.C., Balasubramani, R.: Preparation and antibacterial application of hydroxyapatite doped silver nanoparticles derived from chicken bone. J. King Saud Univ.- Sci. **34**(2), 101749 (2022)
14. Ramesh, S., Loo, Z.Z., Tan, C.Y., Kelvin Chew, W.J., Ching, Y.C., Tarlochan, F., Hari, C., Krishnasamy, S., Bang, L.T., Sarhan, A.A.D.: Characterization of biogenic hydroxyapatite derived from animal bones for biomedical applications. Ceram. Int. **44**(9), 10525–10530 (2018)

15. Bee, S.L., Abdul Hamid, Z.A.: Characterization of chicken bone waste-derived hydroxyapatite and its functionality on chitosan membrane for guided bone regeneration. Compos. Part B **163**, 562–573 (2019)
16. Monıka, Š, Gražyna, S.M., Zbyněk, S.: Bioapatite made from chicken femur bone. Ceramics – Silikáty **55**, 3 (2011)
17. Demirkol, N., Oral, A.Y., Oktar, F.N., Kayali, E.S.: Effects of Commercial Inert Glass (CIG) Addition on Mechanical and Microstructural Properties of Chicken Hydroxyapatite (CHA). Key Eng. Mater. **587**, 33–38 (2014)
18. Kokubo, T., Kim, H.M., Kawashita, M.: Novel bioactive materials with different mechanical properties. Biomaterials **24**, 2161–2175 (2013)
19. Pratap Reddy, M., Venugopal, A., Subrahmanyam, M.: Hydroxyapatite-supported Ag-TiO_2 as Escherichia coli disinfection photocatalyst. Water Res. **41**, 379–386 (2007). https://doi.org/10.1016/j.watres.2006.09.018
20. de Paula Miranda, R.B., Miranda Junior, W.G., Ricci Lazar, D.R., Ussui, V., Marchi, J., Cesar, P.F.: Effect of titania content and biomimetic coating onthe mechanical properties of the Y-TZP/TiO_2 composite. Dent. Mater. **34**(238), 245 (2018). https://doi.org/10.1016/j.dental.2017.11.003
21. Hara, S., Jumpei Aisu, Yu., Nishizaki, H.K., Sanae, G., Kurebayashi, S., Shimizu, S., Ikake, H.: Bulk structure of poly (ethylene glycol)/Titania hybrid system and the evaluation of their influence on apatite growth using simulated body fluid (SBF). Polym. Testing **94**, 106984 (2021). https://doi.org/10.1016/j.polymertesting.2020.106984
22. Khattab, R.M., Badr, H.A., Zawrah, M.F.: Effect of processing techniques on properties of porous TiO_2 and TiO_2/hydroxyapatite composites. Ceram. Int. **44**(7), 8643–8649 (2018)
23. Oktar, F.N.: Hydroxyapatite-TiO_2 composites. Mater. Lett. **60**(17–18), 2207–2210 (2006)
24. Singh, N., Chakraborty, R., Gupta, R.K.: Mutton bone derived hydroxyapatite supported TiO_2 nanoparticles for sustainable photocatalytic applications. J. Environ. Chem. Eng. **6**(1), 459–467 (2018)
25. Pazarlioglu, S., Algan, O., Isikogullari, Ah.M., Gokce, H.: The effect of lanthanum addition on the microstructure and mechanical properties of Mg-modified hydroxyapatite ceramics. Process. Appl. Ceram. **15**(3), 226–237 (2021). https://doi.org/10.2298/PAC2103226P
26. Pazarlioglu, S.S., Salman, S.: The effect of alumina additive and sintering temperature on the microstructural, physical, mechanical, and bioactivity properties of hydroxyapatite–alumina composites. J. Aust. Ceram. Soc. **56**, 413–431 (2020). https://doi.org/10.1007/s41779-019-00345-3
27. Gulsoy, H.O., Pazarlioglu, S., Gulsoy, N., Gundede, B., Mutlu, O.: Effect of Zr, Nb and Ti addition on injection molded 316L stainless steel for bio-applications: Mechanical, electrochemical and biocompatibility properties. J. Mech. Behav. Biomed. Mater. **51**, 215–224 (2015)
28. Herliansyah, M.K., Hamdi, M., Ide-Ektessabi, A., Wildan, M.W., Toque, J.A.: The influence of sintering temperature on the properties of compacted bovine hydroxyapatite. Mater. Sci. Eng., C **29**(5), 1674–1680 (2009). https://doi.org/10.1016/j.msec.2009.01.007
29. Sofronia, A.M., Baies, R., Anghel, E.M., Marinescu, C.A., Tanasescu, S.: Thermal and structural characterization of synthetic and natural nanocrystalline hydroxyapatite. Mater. Sci. Eng., C **43**, 153–163 (2014). https://doi.org/10.1016/j.msec.2014.07.023
30. St. Pierre, P.D.S.: A note on the melting point of titanium dioxide. J. Am. Ceram. Soc. **35**(7), 188 (1952). https://doi.org/10.1111/j.1151-2916.1952.tb13097.x
31. Bulina, N.V., Makarova, S.V., Baev, S.G., Matvienko, A.A., Gerasimov, K.B., Logutenko, O.A., Bystrov, V.S.: A study of thermal stability of hydroxyapatite. Minerals **11**, 1310 (2021). https://doi.org/10.3390/min11121310
32. Nie, J., Zhou, J., Huang, X., Wang, L., Liu, G., Cheng, J.: Effect of TiO_2 doping on densification and mechanical properties of hydroxyapatite by microwave sintering. Ceram. Int. **45**(11), 13647–13655 (2019). https://doi.org/10.1016/j.ceramint.2019.04.007
33. Yim, S., Park, I., Park, J.: Sintering behavior, mechanical properties, and biocompatibility of TiO_2-Co-calcium phosphates composites prepared by AROS process. Mater. Chem. Phys. **252**, 123255 (2020). https://doi.org/10.1016/j.matchemphys.2020.123255
34. Albayrak, O., El-Atwani, O., Altintas, S.: Hydroxyapatite coating on titanium substrate by electrophoretic deposition method: effects of titanium dioxide inner layer on adhesion strength and hydroxyapatite decomposition. Surf. Coat. Technol. **202**(11), 2482–2487 (2008)
35. Sugiyama, K., Takéuchi, Y.: The crystal structure of rutile as a function of temperature up to 1600° C. Z. Kristallogr.- Cryst. Mater. **194**(1–4), 305–314 (1991). https://doi.org/10.1524/zkri.1991.194.14.305
36. Patil, B.M., Wadhawa, G.C., Chaskar, A.C., Walke, P.S.: Low temperature synthesis and thermal expansion study of nanocrystalline $CaTiO_3$. Mater. Lett. **333**, 133627 (2023). https://doi.org/10.1016/j.matlet.2022.133627
37. Pazarlioglu, S.Ü.L.E.Y.M.A.N., Salman, S.E.R.D.A.R.: Effect of yttria on thermal stability, mechanical and in vitro bioactivity properties of hydroxyapatite/alumina composite. J. Ceram. Process. Res. **20**(1), 99–112 (2019)
38. Guidara, A., Chaari, K., Fakhfakh, S., Bouaziz, J.: The effects of MgO, ZrO2 and TiO2 as additives on microstructure and mechanical properties of Al2O3-Fap composite. Mater. Chem. Phys. **202**, 358–368 (2017)
39. Muralithran, G., Ramesh, S.: The effects of sintering temperature on the properties of hydroxyapatite. Ceram. Int. **26**, 221–230 (2000)
40. Hoepfner, T.P., Case, E.D.: The influence of the microstructure on the hardness of sintered hydroxyapatite. Ceram. Int. **29**, 699–706 (2003)
41. Ruys, A.J., Wei, M., Sorrell, C.C., Dickson, M.R., Brandwood, A., Milthome, B.K.: Sintering effects on the strength hydroxyapatite. Biomaterials **16**, 409–415 (1995)
42. Ramesh, S., Tan, C.Y., Tolouei, R., Amiriyan, M., Purbolaksono, J., Sopyan, I., Teng, W.D.: Sintering behavior of hydroxyapatite prepared from different routes. Mater. Des. **34**, 148–154 (2012)
43. Pazarlıoglu, S., Salman, S.: Sintering effect on the microstructural, mechanical, and in vitro bioactivity properties of a commercially synthetic hydroxyapatite. J. Aust. Ceram. Soc. **53**, 391–401 (2017)
44. Rahavi, S., Monshi, A., Emadi, R., Doostmohammadi, A., Akbarian, H.: Determination of crystallite size in synthetic and natural hydroxyapatite: A comparison between XRD and TEM results. Adv. Mater. Res. **620**, 28–34 (2012)
45. Wu, S.C., Hsu, H.C., Hsu, S.K.: Effects of calcination on synthesis of hydroxyapatite derived from oyster shell powders. J. Aust. Ceram. Soc. **55**, 1051–1058 (2019)
46. Royer, A., Viguie, J.C., Heughebaert, M., Heughebaert, J.C.: Stoichiometry of hydroxyapatite: Influence on the flexural strength. J. Mater. Sci. - Mater. Med. **4**, 76–82 (1993). https://doi.org/10.1007/BF00122982
47. Pazarlioglu, S.S.: The effect of alpha-lithium aluminate incorporation on the properties of bovine bone-derived hydroxyapatite. J. Aust. Ceram. Soc. **58**, 1585–1601 (2022). https://doi.org/10.1007/s41779-022-00796-1
48. Shaly, A.A., Priya, G.H., Mahendiran, M., Linet, J.M., Mani, J.A.M.: An intrinsic analysis on the nature of alumina (Al_2O_3) reinforced hydroxyapatite nanocomposite. Phys. B: Condensed Matter **642**(1), 414100 (2022)

49. Shiw, S.L., Pan, W.: Machinable Ti_3SiC_2/hydroxyapatite bioceramic composites by sparkplasma sintering. J. Am. Ceram. Soc. **90**(10), 3331–3333 (2007)
50. Xiaoheng, G., Xiao, L., Huichang, G., Xuetao, S., Naru, Z., Yingjun, W.: Hydrothermal growth of whitlockite coating on β-tricalcium phosphate surfaces for enhancing bone repair potential. J. Mater. Sci. Technol. **34**(6), 1054–1059 (2018)
51. Seo, D.S., Kim, Y.G., Hwang, K.G., Lee, J.K.: Preparation of Hydroxyapatite Powder from Tuna Bone and Its Sinterability Property. J. Korean Ceram. Soc. **45**, 10 (2008)
52. Kutbay, I., Yilmaz, B., Evis, Z., Usta, M.: Effect of calcium fluoride on mechanical behavior and sinterability of nano-hydroxyapatite and titania composites. Ceram. Int. **40**(9), 14817–14826 (2014)
53. Sinusaite, L., Renner, A. M., Schuetz, M. B., Antuzevics, A., Rogulis, U., Grigoraviciute-Puroniene, I., ..., Zarkov, A.: Effect of Mn doping on the low-temperature synthesis of tricalcium phosphate (TCP) polymorphs. J. Eur Ceram. Soc. **39**(10), 3257–3263 (2019)
54. Morejón Alonso, L., Coelho, W. T. G., Santos, L. A. D.: Dual setting α-tricalcium phosphate composite cement obtained by 3d printing. Revista CENIC ciencias químicas [recurso eletrônico]. La Habana, Cuba. **46**(1), 62–65 (2015)
55. Takahashi, K., Fujishiro, Y., Yin, S., Sato, T.: Preparation and compressive strength of α-tricalcium phosphate based cement dispersed with ceramic particles. Ceram. Int. **30**(2), 199–203 (2004)
56. Mimi, M.M., Haque, M.R., Hasan, M.R.: effect of addition of cao on compressive strength of high-volume fly ash concrete. J. Civ. Eng. Sci. Technol. **14**(1), 64–76 (2023)
57. Szewczyk-Nykiel, A., Nykiel, M.: Analysıs of the sintering process of 316l–hydroxyapatite composite biomaterials. Technical Transactions Mechanics **79** (2015)
58. Suchanek, W., Yashima, M., Kakihana, M., Yoshimura, M.: Hydroxyapatite ceramics with selected sintering additives. Biomaterials **18**(13), 923–933 (1997)
59. Ryu, H.S., Youn, H.J., Hong, K.S., Chang, B.S., Lee, C.K., Chung, S.S.: An improvement in sintering property of β-tricalcium phosphate by addition of calcium pyrophosphate. Biomaterials **23**(3), 909–914 (2002)
60. Ramirez-Gutierrez, C.F., Londoño-Restrepo, S.M., Del Real, A., Mondragón, M.A., Rodriguez-García, M.E.: Effect of the temperature and sintering time on the thermal, structural, morphological, and vibrational properties of hydroxyapatite derived from pig bone. Ceram. Int. **43**(10), 7552–7559 (2017)
61. Maroua, T., Ibrahim, A., Algarni, H., Ayed, F.B., Yousef, E.S.: Mechanical and tribological properties of the tricalcium phosphate-magnesium oxide composites. Mater. Sci. Eng. C **96**, 716–729 (2019)
62. Nie, J., Zhou, J., Huang, X., Wang, L., Liu, G., Cheng, J.: Effect of TiO_2 doping on densification and mechanical properties of hydroxyapatite by microwave sintering. Ceram. Int. **45**(11), 13647–13655 (2019)
63. Guidara, A., Chaari, K., Fakhfakh, S., Bouaziz, J.: The effects of MgO, ZrO_2 and TiO_2 as additives on microstructure and mechanical properties of Al_2O_3-FAp composite. Mater. Chem. Phys. **202**, 358–368 (2017)
64. Hannora, A.E., Ataya, S.: Structure and Compression Strength of Hydroxyapatite/Titania Nanocomposites Formed by High Energy Mall Milling. J. Alloys Compd. **658**, 222–233 (2016)
65. Wu, J.M.: Low-temperature preparation of anatase and rutile layers on titanium substrates and their ability to induce in vitro apatite deposition. J. Am. Ceram. Soc. **87**, 9 (2004)
66. Auger, M.A., Savoini, B., Muňoz, A., Leguey, T., Monge, M.A., Pareja, R., Victoria, J.: Mechanical characteristics of porous hydroxyapatite/oxide composites produced by post-sintering hot isostatic pressing. Ceram. Int. **35**, 2373–2380 (2009). https://doi.org/10.1016/j.ceramint.2009.01.016
67. Tronco, M.C., Cassel, J.B., dos Santos, L.A.: α-TCP-based calcium phosphate cements: A critical review. Acta Biomater. **151**, 70–87 (2022)
68. Qin, T., Li, X., Long, H., Bin, S., Xu, Y.: Bioactive tetracalcium phosphate scaffolds fabricated by selective laser sintering for bone regeneration applications. Materials **13**(10), 2268 (2020)
69. Lindberg, F., Heinrichs, J., Ericson, F., Thomsen, P., Engqvist, H.: Hydroxylapatite growth on single-crystal rutile substrates. Biomaterials **29**(23), 3317–3323 (2008)
70. Macon, A. L., Kim, T. B., Valliant, E. M., Goetschius, K., Brow, R. K., Day, D. E., ..., Jones, J. R.: A unified in vitro evaluation for apatite-forming ability of bioactive glasses and their variants. J. Mater. Sci.: Mater. Med. **26**, 1–10 (2015). https://doi.org/10.1007/s10856-015-5403-9
71. Narayanan, R., Lee, H.J., Kwon, T.Y., Kim, K.H.: Anodic TiO2 nanotubes from stirred baths: hydroxyapatite growth & osteoblast responses. Mater. Chem. Phys. **125**(3), 510–517 (2011)
72. Zheng, X.B., Ding, C.X.: Characterization of plasma-sprayed hydroxyapatite/TiO_2 composite coatings. J Therm Spray Tech **9**, 520–525 (2011). https://doi.org/10.1007/BF02608556
73. Yajing, Y., Qiongqiong, D., Yong, H., Han, S., Pang, X.: Magnesium substituted hydroxyapatite coating on titanium with nanotublar TiO2 intermediate layer via electrochemical deposition. Appl. Surf. Sci. **305**, 77–85 (2014)

Publisher's Note Springer Nature remains neutral with regard to jurisdictional claims in published maps and institutional affiliations.